JACS
JOURNAL OF THE AMERICAN CHEMICAL SOCIETY

COMMUNICATION

pubs.acs.org/JACS

Molecule and Electron Transfer through Coordination-Based Molecular Assemblies

Leila Motiei, Revital Kaminker, Mauro Sassi, and Milko E. van der Boom*

Department of Organic Chemistry, The Weizmann Institute of Science, Rehovot 76100, Israel

Supporting Information

ABSTRACT: This study provides insight into the internal structure of surface-confined molecular assemblies. The permeability of the layer-by-layer grown thin films can be controlled systematically by varying their composition and the structure of their molecular components. Moreover, the thickness can be used to control molecule permeation versus electron transfer.

The rational design, preparation, and properties of porous materials might lead to new applications in energy storage, separation of gases, heterogeneous catalysis, and sensing.[1,2] Size-selective transport of small molecules has been achieved with surface-confined materials having cavities that reflect their molecular dimensions.[3,4] However, controlling pore structures and understanding their size-exclusion properties remain a challenge.[5] Equally important are the electron transfer (ET) properties of surface-confined molecular materials. Both bioinspired and small-molecule-based systems have undergone tremendous progress.[6,7] The present study shows that the permeability of layer-by-layer grown molecular assemblies (MAs) can be controlled by varying their composition and the structure of their molecular components. Moreover, the thickness of the coordination-based MAs can be used to direct molecule permeation versus ET.

We recently reported on the formation of surface-confined MAs, which involves iterative wet-chemical deposition of a $PdCl_2$ salt and vinylpyridine-based chromophores,[8] including compounds **1** and **2** (Scheme 1A).[9−11] The MAs used in this study consisted of the organic chromophore **1** (**MA1**),[9] the ruthenium polypyridyl complex **2** (**MA2**),[10] or a combination of the two (**MA3**).[11] These MAs were formed on indium tin oxide (ITO)-coated glass slides functionalized with a pyridyl-terminated template layer [Scheme S1 in the Supporting Information (SI)]. The molecular-sieving properties[12] of 5 and 20 nm thick MAs were assessed by measuring the cyclic voltammetric responses of four redox probes having different sizes (compounds **3**−**6** in Scheme 1B); the results are shown in Table S1 in the SI. Representative cyclic voltammograms of probes **4** and **5** obtained using 5 and 20 nm thick structures of **MA1** and **MA2** on ITO are shown in Figure 1. The relatively small dimethoxybenzoquinone (**3**) (Figure S1 in the SI) and 2,3-dibromo-1,4-naphthoquinone (**4**) penetrate the MAs regardless of their thickness and are directly electrochemically addressed by the ITO electrode. Selectivity was observed with the larger probe, 3,3′,5,5′-tetra-*tert*-butyldiphenoquinone (**5**). This quinone **5** does not traverse

Scheme 1. Molecular Structures of (A) Compounds 1 and 2 Used To Form Three Molecular Assemblies (MAs) Cross-Linked with $PdCl_2$ ($1\cdot PdCl_2$ = MA1;[9] $2\cdot PdCl_2$ = MA2;[10] $1\cdot PdCl_2 + 2\cdot PdCl_2$ = MA3[11]) and (B) Redox Probes 3−6

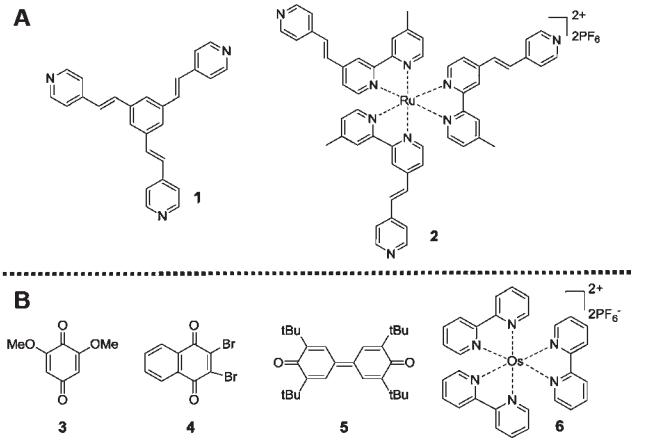

MA1-[**5 nm**], demonstrating that the pore size of this assembly lies somewhere between the molecular dimensions of probes **4** and **5**. Furthermore, we observed that probe **5** does traverse **MA2**-[**5 nm**]. These results show that the different structures of the molecular components (**1** and **2**) are expressed by the porosity of the MAs. Size selectivity was also achieved with **MA2** upon increasing its thickness from 5 to 20 nm. **MA2**-[**20 nm**] was still permeable for the small probes (**3** and **4**); however, probe **5** could not traverse this thicker interface. The probe size cutoff for **MA1**-[**5 nm**] and **MA2**-[**20 nm**] is now the same under identical reaction conditions. It is known that permeation varies inversely with film thickness.[13,14] In addition, thicker films might contain fewer defects and allow size-selective discrimination of molecules.[15] One could conjecture that our probes can reach the ITO electrode by diffusing through pinholes or defects.[16] However, the observed selectivity rules out this possibility because mass transport through pinholes or film imperfections is believed to be independent of the dimensions of the diffusing molecules.[4,13]

Figure 2 shows cyclic voltammograms for 5 and 20 nm thick structures of **MA2** and **MA3** with probe **6**. Both **MA2**-[**5 nm**] and **MA3**-[**5 nm**] were still sufficiently porous for probe **6** to reach the ITO surface. The distorted wave shapes arose from the diffusive nature of the mass transport, which was also reflected in the linear dependence ($R^2 = 0.99$) of the peak currents versus the

Received: July 4, 2011
Published: August 16, 2011

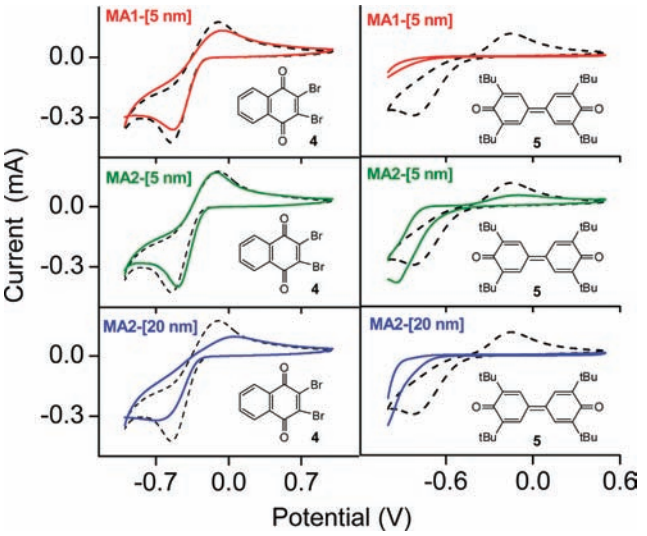

Figure 1. Representative cyclic voltammograms of quinones **4** (1.3 mM) and **5** (1.3 mM) obtained using ITO electrodes (0.7 cm × 1 cm) functionalized with **MA1**-[**5 nm**], **MA2**-[**5 nm**], or **MA2**-[**20 nm**]. The scan rate was 100 mV s^{-1}. The black dashed lines denote the voltammetric responses using bare ITO electrodes. These experiments were carried out at room temperature in dry 0.05 M $TBABF_4/CH_3CN$ under N_2. ITO-coated glass, Pt wire, and Ag/AgCl were used as the working, counter, and reference electrodes, respectively. The thickness of the molecular assemblies (MAs) was estimated by ellipsometry using silicon substrates.

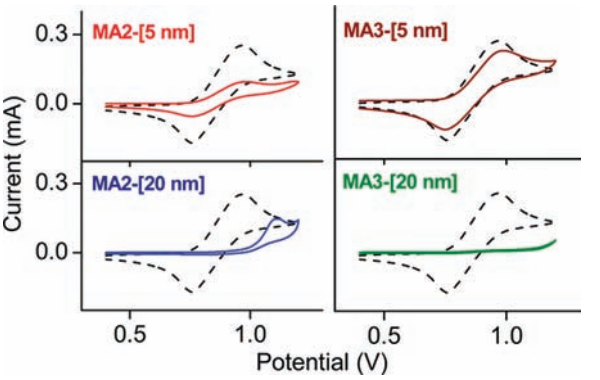

Figure 2. Representative cyclic voltammograms vs Ag/AgCl of probe **6** (0.7 mM) using ITO substrates (0.7 cm × 1 cm) functionalized with **MA2**-[**5 nm**], **MA2**-[**20 nm**], **MA3**-[**5 nm**], or **MA3**-[**20 nm**]. The measurements were performed in dry 0.05 M $TBABF_4/CH_3CN$ at a scan rate of 100 mV s^{-1}. The black dashed lines denote the voltammetric response of probe **6** using bare ITO electrodes.

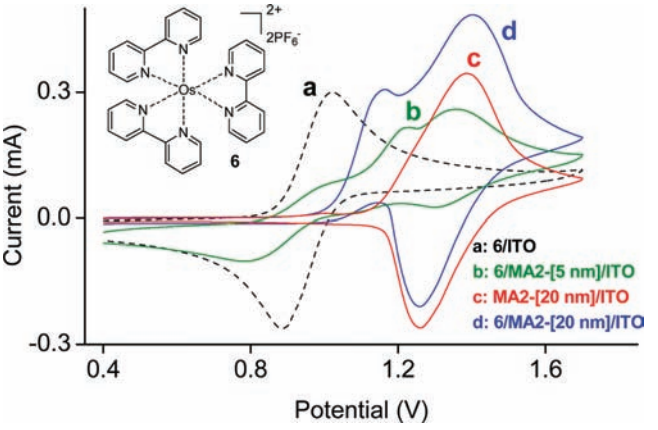

Figure 3. Representative cyclic voltammograms vs Ag/AgCl of (a, b, d) probe **6** (0.7 mM) using (a) a bare ITO electrode (0.7 cm × 1 cm) and ITO substrates functionalized with (b) **MA2**-[**5 nm**] and (d) **MA2**-[**20 nm**]. (c) Cyclic voltammogram of **MA2**-[**20 nm**] on ITO without probe **6**. The measurements were performed in dry 0.05 M $TBABF_4/CH_3CN$ at a scan rate of 100 mV s^{-1}.

square root of the scan rate (100−900 mV s^{-1}; Figure S2). There is some difference between these two MAs. The relative intensity of the current for probe **6** in the presence of **MA3**-[**5 nm**] was larger than that of **MA2**-[**5 nm**], reflecting the presence of higher porosity/larger pores in **MA3**-[**5 nm**]. Size selectivity was also achieved for these interface/probe combinations when the thickness of these two MAs was increased from 5 to 20 nm. The permeation of probe **6** was suppressed by both **MA2**-[**20 nm**] and **MA3**-[**20 nm**]. Electrostatic repulsion (Donnan exclusion) did not seem to play a significant role,[17] since the electrolyte concentration (0.05−1.0 M $TBABF_4$) did not affect the permeability of **MA2**-[**5 nm**] and **MA2**-[**20 nm**] toward the cationic probe **6** (Figure S3).

ET between redox probes and functionalized electrodes might involve[18] (I) a diffusional pathway, where a probe reacts at the ITO electrode−MA interface or (II) a charge-transfer pathway, where the probe is oxidized at the MA−solution interface. Our aforementioned observations with the various probe/MA combinations show that pathway I operates, since both oxidative and reductive components of the voltammetric waves of the probes were observed. For pathway II, the charge transfer should involve the MA and irreversible oxidation of the probe, which occurs at or near an anodic wave of the modified electrode. Blocking pathway I redirects the electrochemical addressing of the probe at the ITO surface to a MA-mediated ET process. For example, the cyclic voltammogram of probe **6** recorded with a bare ITO electrode shows a reversible redox process characteristic of an $Os^{2+/3+}$ couple with $E_{1/2}$ = 0.95 V (black dashed line a in Figure 3). In contrast, the cyclic voltammogram of probe **6** recorded with an ITO electrode functionalized with **MA2**-[**5 nm**] shows three discrete charge-transfer processes (Figure 3, line b). The first oxidation peak, E_{ox} = 0.98 V, can be assigned to a direct ET process between probe **6** and the ITO electrode. The presence of the oxidation peak at 1.20 V is related to the indirect oxidation of probe **6** by the surface-confined ruthenium centers in **2** at the **MA2**-[**5 nm**]−solution interface. The peak at E_{ox} = 1.35 V represents the oxidation of the ruthenium complexes **2** in **MA2**-[**5-nm**]. The redox-active **MA2** and **MA3** exhibit well-defined electrochemical responses with a half-wave redox potential of $E_{1/2} \approx$ 1.3 V vs Ag/AgCl, which is characteristic of the $Ru^{2+/3+}$ redox couple (Figure 3, red line c; also see Figure S4). For the thicker **MA2**-[**20 nm**] films, probe **6** does not reach the ITO electrode surface during the time scale of the experiment, and its oxidation occurs by a charge-transfer pathway involving **MA2**-[**20 nm**] (Figure 3, blue line d). The increase in the anodic wave and the corresponding decrease in the cathodic wave are indicative of concurrent electrocatalytic oxidation of probe **6** by the ruthenium complexes **2**.[19]

Our observations are consistent with the growth processes of the MAs and their electrochemical properties.[7,9−11,20] **MA1** is formed linearly with the number of organic chromophore **1** and $PdCl_2$ deposition cycles.[9] **MA2** and **MA3** exhibit exponential

growth.[10,11,21] These two self-propagating molecular assemblies (SPMAs) can store palladium and use it to form additional "layers". In contrast, **MA1** is not a reservoir for metal salts.[10,21] This striking difference might be caused by the internal MA structures. **MA2** and **MA3** have (i) higher porosity (more voids), (ii) more interconnectedness of pores (the existence of percolation pathways), and/or (iii) higher pore diameters (leading to lower constrictivity). **MA1** is less porous and therefore has a lower permeability. For instance, the relatively large probe **5** does not traverse **MA1**-[**5 nm**], but it reaches the ITO electrode coated with **MA2**-[**5 nm**]. The permeability of **MA2** is somewhat comparable to that of the hybrid **MA3**, indicating that compound **2** dominates the overall structure and the molecular-sieving properties of **MA3**.

In conclusion, this study provides new fundamental insight into the internal structure of layer-by-layer grown MAs[9−11] that is not readily attainable otherwise. Size-selective permeation of small molecules has been demonstrated electrochemically using 5 and 20 nm thick coordination-based membranes. This process can be controlled by varying (i) the molecular structures of the MAs or (ii) the thickness of the MA. Blocking the ITO electrode surface can mediate an exclusive ET pathway, as shown for **MA2** and probe **6**. Transition-metal-directed assembly can be used to control voids, as shown by Stang and Fujita.[22] The fact that redox-active interfaces can be generated with control over mass and electron transfer processes might lead to the design of conceptually new sensors and storage/release chemistry.

■ ASSOCIATED CONTENT

Supporting Information. Structures of the pyridyl-terminated templates (Scheme S1) and electrochemical data (Figures S1−S4 and Table S1). This material is available free of charge via the Internet at http://pubs.acs.org.

■ AUTHOR INFORMATION

Corresponding Author
milko.vanderboom@weizmann.ac.il

■ ACKNOWLEDGMENT

This research was supported by the Minerva Foundation and the Helen and Martin Kimmel Center for Molecular Design. We thank Dr. Michal Lahav (WIS) for fruitful discussions. M. E. van der Boom is the incumbent of the Bruce A. Pearlman Professorial Chair in Synthetic Organic Chemistry.

■ REFERENCES

(1) (a) Shekhah, O.; Liu, J.; Fischer, R. A.; Wöll, Ch. *Chem. Soc. Rev.* **2011**, *40*, 1081. (b) D'Alessandro, D. M.; Smit, B.; Long, J. R. *Angew. Chem., Int. Ed.* **2010**, *49*, 6058. (c) Roques, N.; Mugnaini, V.; Veciana, J. *Top. Curr. Chem.* **2010**, *293*, 207.

(2) (a) Furukawa, H.; Ko, N.; Go, Y. B.; Aratani, N.; Choi, S. B.; Choi, E.; Yazaydin, A. O.; Snurr, R. Q.; O'Keeffe, M.; Kim, J.; Yaghi, O. M. *Science* **2010**, *329*, 424. (b) Striemer, C. C.; Gaborski, T. R.; McGrath, J. L.; Fauchet, P. M. *Nature* **2007**, *445*, 749. (c) Maji, T. K.; Matsuda, R.; Kitagawa, S. *Nat. Mater.* **2007**, *6*, 142. (d) Davis, M. E. *Nature* **2002**, *417*, 813.

(3) (a) Williams, M. E.; Benkstein, K. D.; Abel, C.; Dinolfo, P. H.; Hupp, J. T. *Proc. Natl. Acad. Sci. U.S.A.* **2002**, *99*, 5171. (b) Pyati, R.; Murray, R. W. *J. Phys. Chem.* **1994**, *98*, 11129.

(4) (a) Motesharei, K.; Ghadiri, M. R. *J. Am. Chem. Soc.* **1997**, *119*, 11306. (b) Gould, S.; Gray, K. H.; Linton, R. W.; Meyer, T. J. *J. Phys. Chem.* **1995**, *99*, 16052.

(5) Zhao, D.; Timmons, D. J.; Yuan, D.; Zhou, H.-C. *Acc. Chem. Res.* **2011**, *44*, 123.

(6) (a) Genereux, J. C.; Wuerth, S. M.; Barton, J. K. *J. Am. Chem. Soc.* **2011**, *133*, 3863. (b) Kurita, T.; Nishimori, Y.; Toshimitsu, F.; Muratsugu, S.; Kume, S.; Nishihara, H. *J. Am. Chem. Soc.* **2010**, *132*, 4524. (c) Ron, I.; Pecht, I.; Sheves, M.; Cahen, D. *Acc. Chem. Res.* **2010**, *43*, 945. (d) Tuccitto, N.; Ferri, V.; Cavazzini, M.; Quici, S.; Zhavnerko, G.; Licciardello, A.; Rampi, M. A. *Nat. Mater.* **2009**, *8*, 41. (e) Katz, E.; Lioubashevsky, O.; Willner, I. *J. Am. Chem. Soc.* **2004**, *126*, 15520. (f) Long, Y.-T.; Li, C.-Z.; Sutherland, T. C.; Chahma, M.; Lee, J. S.; Kraatz, H.-B. *J. Am. Chem. Soc.* **2003**, *125*, 8724. (g) Hong, H. G.; Mallouk, T. E. *Langmuir* **1991**, *7*, 2362.

(7) Motiei, L.; Lahav, M.; Gulino, A.; Iron, M. A.; van der Boom, M. E. *J. Phys. Chem. B* **2010**, *114*, 14283.

(8) Altman, M.; Shukla, A. D.; Zubkov, T.; Evmenenko, G.; Dutta, P.; van der Boom, M. E. *J. Am. Chem. Soc.* **2006**, *128*, 7374.

(9) Kaminker, R.; Motiei, L.; Gulino, A.; Fragalà, I.; Shimon, L. J. W.; Evmenenko, G.; Dutta, P.; Iron, M. A.; van der Boom, M. E. *J. Am. Chem. Soc.* **2010**, *132*, 14554.

(10) Choudhury, J.; Kaminker, R.; Motiei, L.; de Ruiter, G.; Morozov, M.; Lupo, F.; Gulino, A.; van der Boom, M. E. *J. Am. Chem. Soc.* **2010**, *132*, 9295.

(11) Motiei, L.; Sassi, M.; Kaminker, R.; Evmenenko, G.; Dutta, P.; Iron, M. A.; van der Boom, M. E. *Langmuir* **2011**, *27*, 1319.

(12) (a) Beck, R. E.; Schultz, J. S. *Science* **1970**, *170*, 1302. (b) Renkin, E. M. *J. Gen. Physiol.* **1954**, *38*, 225.

(13) Bélanger, S.; Hupp, J. T.; Stern, C. L.; Slone, R. V.; Watson, D. F.; Carrell, T. G. *J. Am. Chem. Soc.* **1999**, *121*, 557.

(14) (a) Robeson, L. M. *J. Membr. Sci.* **1991**, *62*, 165. (b) Freeman, B. D. *Macromolecules* **1999**, *32*, 375.

(15) Bélanger, S.; Stevenson, K. J.; Mudakha, S. A.; Hupp, J. T. *Langmuir* **1999**, *15*, 837.

(16) Finklea, H. O. *Electroanal. Chem.* **1996**, *19*, 110.

(17) (a) Elliott, J. M.; Cabuché, L. M.; Bartlett, P. N. *Anal. Chem.* **2001**, *73*, 2855. (b) Krasemann, L.; Tieke, B. *Langmuir* **2000**, *16*, 287.

(18) (a) Palomaki, P. K. B.; Krawicz, A.; Dinolfo, P. H. *Langmuir* **2011**, *27*, 4613. (b) Hillebrandt, H.; Tanaka, M. *J. Phys. Chem. B* **2001**, *105*, 4270. (c) Nishihara, H.; Noguchi, M.; Aramaki, K. *Inorg. Chem.* **1987**, *26*, 2862. (d) Ellis, C. D.; Murphy, W. R., Jr.; Meyer, T. J. *J. Am. Chem. Soc.* **1981**, *103*, 7480.

(19) Deronzier, A.; Moutet, J.-C. *Coord. Chem. Rev.* **1996**, *147*, 339.

(20) The porosity of the MAs can result in an underestimation of attenuation factors, as proposed in ref 7.

(21) Motiei, L.; Altman, M.; Gupta, T.; Lupo, F.; Gulino, A.; Evmenenko, G.; Dutta, P.; van der Boom, M. E. *J. Am. Chem. Soc.* **2008**, *130*, 8913.

(22) (a) Li, S. S.; Northrop, B. H.; Yuan, Q. H.; Wan, L. J.; Stang, P. J. *Acc. Chem. Res.* **2009**, *42*, 249. (b) Fujita, M.; Ogura, K. *Coord. Chem. Rev.* **1996**, *148*, 249.